# An Application of the IMC Software to Controller Design for the JPL LSCL Experiment Facility

Guoming Zhu and Robert E. Skelton

Space Systems Control Laboratory
1293 Potter Engineering Center
Purdue University
West Lafayette, IN 47907

## ABSTRACT

A software package which Integrates Model reduction and Controller design (The IMC software) is applied to design controllers for the JPL Large Spacecraft Control Laboratory Experiment Facility. Modal Cost Analysis is used for the model reduction, and various Output Covariance Constraints are guaranteed by the controller design. The main motivation is to find the controller with the "best" performance with respect to output variances. Indeed it is shown that by iterating on the reduced order design model, the controller designed does have better performance than that obtained with the first model reduction.

## 1. INTRODUCTION

The objective of this research is to develop controller design software IMC (Integrated Modeling and Control) for a realistic flexible space structure control problem. The main interests are two-fold: i) the design of high performance fixed order dynamic controllers for this complex structure, and ii) to test the efficacy of the IMC software for the search of the controller with the "best" performance, among all model based controllers.

Almost all available controller design techniques are based upon a given model of the physical plant. In general, perfect models are impossible to construct. Modeling error exists in every mathematical model used for control design. There are three ways to deal with modeling error in a controller design procedure. First, one may use robust control theory. The controller designed with robust control theory is tolerant to a specified set of modeling errors. But a poor model may lead to a poor controller even if the controller is robust with respect to the given model. Second, one may treat the modeling and controller design as a combined problem, and try to refine the design model to find one that is "appropriate" for controller design in the sense of best closed loop operation. The third method is adaptive control which intends to adjust the controller in real-time to compensate for modeling errors.

From our experience a *nominal* controller design procedure based on an "appropriate" model may yield better performance than a *robust* controller that is based on an poor model (say, given by finite element modeling or identification). Hence, we use the second method to obtain a design model that is more compatible to the particular controller design than the other two methods.

In this research the integrated design procedure is applied to design controllers for the LSCL Experiment Facility. Assuming that a "true enough" high order mathematical model can be obtained by some modeling method (analytical or by identification), our procedure reduces the "true enough" model (we shall call this the "evaluation model") to an order appropriate for full order controller design based on the reduced order model. Repeating the model reduction and controller design by using *closed* loop information such that the process is convergent, the integrated procedure produces a design model "appropriate" to the corresponding controller.

The model reduction technique used in this experiment is the Modal Cost Analysis (MCA) which calculates each modal contribution $V_i$ to a weighted quadratic cost function [7-9].

$$V \triangleq \lim_{k \to \infty} \mathcal{E}\, y^T(k) Q y(k) = \sum_{i=1}^{N} V_i \ , \qquad (1.1)$$

where N is the number of modes in the model. The smallest contribution (smallest $V_i$) indicates the modes to be deleted in the reduced model. Closed form analytical expression of $V_i$ are available, see [8].

Two controller design methods (BOCC and EOL$_\infty$) were applied to this experiment. The BOCC algorithm [1-4] designs controllers minimizing the control effort subject to output covariance constraints (for zero mean white noise input). The BOCC algorithm can be also used to satisfy the output $\ell_\infty$ constraints when the input is an $\ell_2$ disturbance. The EOL$_\infty$ algorithm [5] is an extension of the deterministic interpretation of the BOCC. The EOL$_\infty$ designs controllers to satisfy given output $\ell_\infty$ constraints when the input $\ell_2$ disturbances have an outer product matrix upper bound. The main difference between those two design algorithms is that the BOCC algorithm only iterates on the feedback gain, but the EOL$_\infty$ algorithm iterates on both estimator and control feedback gains. We only present the BOCC results in this paper. The definition and solution of the BOCC and EOL$_\infty$ can be found in [3-5].

There are two iteration loops in the IMC software, one inner loop and one outer, used to realize the integration of model reduction and controller design. The inner loop, called the $\alpha$-loop, intends to obtain the controller for "best" performance (with respect to the *evaluation model*) with the given reduced order model (called the *design model*) by gradually increasing the required performance (smaller variance constraints). The outer loop iterates on the design model to make the design model be "appropriate" to the corresponding controller with the "best" performance.

The paper is organized as follows. Section 2 combines model reduction and controller design techniques which is the main philosophy of the IMC software presented in Section 3. The controller design and test results are presented in Section 4. The last section adds some conclusions.

## 2. INTEGRATION OF MODEL REDUCTION AND CONTROLLER DESIGN

It is well known that finding a good model for control design is a difficult problem because of uncertain parameters, nonlinearity and neglected dynamics of the physical system. It is impossible to separate the modeling and controller design

problems. For example, considering a linear system with a nonlinear actuator, one may apply linear control theory to design a controller. In this case the nonlinear actuator should be linearized at some nominal point, but the nominal point is related to the control signal level of the controller which will be designed after linearization of the actuator model. Consequently, the modeling and controller design problems become an iterative process, see the examples in [6].

In this section we mainly consider the effect of the neglected dynamics of the physical system. We are trying to obtain the "best" performance for a high order given physical system with a fixed order controller. There are at least three ways to find a fixed order controller for a given linear system. The first way is to design a fixed order controller directly. The second is to design a full order controller first and then reduce the controller to the required order. The last one is to reduce the model first and then do the full order control design based on the reduced order model. The advantage of the first method is that the performance of the closed loop system with the designed controller is guaranteed. But unfortunately there exists no closed form for the design of such controllers. Since full order controller design methods are available for most control theories, $H_\infty$, LQG and so on, we will use a variation of the third method, we call *the integration of model reduction and controller design*, to design reduced order controllers.

The integrated design procedure, utilizing Modal Cost Analysis for model reduction and the BOCC or $EOL_\infty$ for controller design, is shown in Figure 1. The design procedure searches for the controller with the "best" performance by tuning the design model until the design model corresponds to the controller with the "best" performance. This procedure is developed under the following basic assumption that the only modeling errors existing in the design model are from the model reduction, i.e., the evaluation model is assumed to be "true enough". This assumption allows us to evaluate the designed controller based on the evaluation model, prior to hardware testing in the lab. Of course, we also compare these analytical results with the experimental results.

The evaluation model in Figure 1 can be obtained either from system identification or from mathematical modeling, e.g., the finite element model combining with the sensor and actuator dynamics. Generally, the size of the evaluation model is too large for controller design. Hence, the model reduction is necessary.

The cost function defined in (1.1) used in the model reduction is the summation of the weighted output variance with respect to the white noise input. Note that the modal cost is very much dependent upon the input and output weighting matrices $\overline{W} = \text{diag}[W, R]$ and Q, where the input weighting matrix $\overline{W}$ is used to compute the output covariance. Hence, the choice of those two matrices will directly effect the model reduction. How to choose Q and $\overline{W}$ is a major subject of this paper. For the first iteration of this experiment, matrix W is the input white noise covariance matrix $W_p$, and Q and R are diagonal matrices whose elements are the inversed square of the hard limitation on inputs and outputs, respectively.

The main philosophy of our $\alpha$-loop in Figure 2 is to obtain a sequence of controllers from low control effort to high. Here $\alpha$ denotes the controller number. The controller sequence is obtained by reducing the required performance specification during controller design.

The main purpose of the BOCC $\alpha$-loop is to obtain the "best" performance with the given (reduced order) *design model* (obtained from MCA model reduction of the *evaluation model*), which is expressed in the following form

$$\left.\begin{aligned} x_p(k+1) &= A_p x_p(k) + B_p u(k) + D_p w_p(k) \\ y_p(k) &= C_p x_p(k) \\ z(k) &= M_p x_p(k) + v(k) \end{aligned}\right\} . \qquad (2.1)$$

The BOCC $\alpha$-loop starts with the evaluation and design models. Suppose that the output $y_p$ can be divided into m output groups $\hat{y}_i$. Let $Y_i(0)$ (i = 1, 2, ..., m) denote the open loop output covariance of the *evaluation model* for output group $\hat{y}_i$, assuming that the open loop system is asymptotically stable. Define $L_i$ (i = 1, 2, ..., m) to be a lower bound of the output covariance of the closed loop system with any full order controller. Hence, any specification which is less than or equal to $L_i$ is unachievable with respect to the design model. Then the specification matrix $\overline{Y}_i(\alpha)$ (i = 1, 2, ..., m) can be generated by the following equation

$$\overline{Y}_i(\alpha) = [Y_i(0) - L_i](1 - \beta)^{\alpha} + L_i \ , \ \alpha = 1, 2, ..., \alpha_m \ , \qquad (2.2)$$

where $0 < \beta < 1$ is a design parameter and $\alpha$ is the integer counter (iteration number for the $\alpha$-loop). Note that the specifications are gradually reduced as $\alpha$ increases. The main reason to use (2.2) to produce specification $\overline{Y}_i(\alpha)$ is to make the *change* of specification small (from one iteration to the next) when it is close to its lower bound $L_i$.

With each set of design specifications $\bar{Y}_i(\alpha)$, the BOCC algorithm will produce a controller with index $\alpha$, called the $\alpha$th controller, using the *design model* (2.1). The closed loop system with the *design model* and the $\alpha$th controller is asymptotically stable because the BOCC controller is an LQG controller with a special choice of the output weighting matrix. But the closed loop system with the *evaluation model* may not be stable. If the closed loop system with respect to the *evaluation model* is unstable, the $\alpha$-loop will be terminated, according to the BOCC $\alpha$-loop diagram in Figure 2, otherwise the output covariance matrices $Y_i^e(\alpha)$ and $Y_i^d(\alpha)$ with respect to the *evaluation* and *design models* will be computed for future use.

Since the open loop system is asymptotically stable, the closed loop system will be asymptotically stable if the controller gain is small enough. As the control gains increase, i.e., $\alpha$ increases, the closed loop system with respect to the *evaluation model* may become unstable. Hence, a plot similar to Figure 3 can be generated for analysis. We use $\alpha_b$ to denote the point with the "best" performance with respect to the evaluation model. The information on the $\alpha_b$th controller will be used for the new model reduction because we want the design model to be "appropriate" to the controller with the "best" performance. The new output and input weighting matrices Q and R will be computed in the following way

$$Q_i = \alpha_q Q_i(\alpha_b) + (1 - \alpha_q)\,|\,\bar{\sigma}[Y_i^e(\alpha_b)] - \bar{\sigma}[Y_i^d(\alpha_b)]\,|\,I_{m_i} \tag{2.3a}$$

$$Q = \text{block diag}[Q_1, Q_2, \ldots, Q_m] \tag{2.3b}$$

and

$$R = \alpha_r R(0) + (1 - \alpha_r)\text{diag}([\ \ldots,\ |U_j^e(\alpha_b) - U_j^d(\alpha_b)|,\ \ldots]) \tag{2.4}$$

where $0 \le \alpha_q \le 1$ and $0 \le \alpha_r \le 1$ are design parameters. R(0) is the controller channel input weighting matrix used in the first MCA model reduction. $U_j^e(\alpha_b)$ and $U_j^d(\alpha_b)$ ($j = 1, 2, \ldots, n_u$) are the closed loop input variances of the $\alpha_b$th controller with respect to the evaluation and design model respectively. Similarly, $Y_i^e(\alpha_b)$ and $Y_i^d(\alpha_b)$ are the output covariances. The main reason to add these items to correct the input and output weighting matrices is to reduce the differences between the evaluation and design models for the $\alpha_b$th controller.

$Q_i(\alpha_b)$ is the convergent output weighting matrix for the ith block during the design of the $\alpha_b$th controller. The importance of $Q_i(\alpha_b)$ can be clearly observed in the OVC problem (a special case of the BOCC problem when each block has dimension

equal to one). It is noted that during the OVC design iteration procedure the output weighting matrix Q is adjusted so that if a particular output specification $\overline{Y}_i$ is not achieved, the corresponding $Q_i$ will be increased according to the discrepancy between the current output variance $Y_i$ and the specification $\overline{Y}_i$. Consequently, those outputs with hard-to-achieve specifications (indicated by $Y_i = \overline{Y}_i$) will end up with large $Q_i$'s, and those with easy-to-achieve specifications ($Y_i < \overline{Y}_i$) will have the small $Q_i$'s. In fact, for those outputs that end up with variances smaller than the corresponding $\overline{Y}_i$'s the final convergent $Q_i$'s will be zero. This implies that these output constraints are not important and can be disregarded during design. However, at the beginning, this information is unknown. As a result, the convergent Q appropriately reflects the importance of each output with respect to the given specification. This property is very helpful for the model reduction using Modal Cost Analysis, because MCA calculates the contribution of each mode to a weighted output cost $\mathcal{E}_{\infty} y^T Q y$ and deletes the least important modes accordingly. Hence, if the weighting matrix can appropriately reflect the importance of each output, then the reduced model using MCA will keep the information which is important to the required performance.

The controller evaluation part mainly evaluates the designed controllers in the $\alpha$-loop study to see whether the performance is satisfactory or not. The evaluation (plot in Figure 3) will provide the information to adjust these design parameters, e.g., $\alpha_q$, $\alpha_r$ and so on, in the $\alpha$-loop study.

As a result, it is clear now that in the integration of model reduction and controller design there are two iterative loops, the Q-loop and $\alpha$-loop. The Q-loop is used to *combine the model reduction and the controller design process* such that at convergence the design model corresponds to the controller with the "best" performance. The $\alpha$-loop intends to *search for the controller of the "best" performance with respect to the evaluation model, and a given design model.*

## 3. THE IMC SOFTWARE

An IMC (Integration of Model reduction and Controller design) software has been developed to integrate the model reduction and controller design process presented in the last section. The IMC software makes it possible to obtain the rapid redesign capability in a workstation environment using MATLAB.

The idea of the integrated procedure of model reduction and controller design was first applied to design controllers for NASA's Minimast at Langley Research Center [10]. The realization of this integrated idea needs a certain amount of computation, and some expert is needed to manage the whole integrated design process. Some parameters must be chosen, and if changed, the whole process must be repeated. In order to reduce the repeated work during the integrated controller design process, we are motivated to put all the independent software modules, e.g., MCA model reduction, OVC, BOCC and $EOL_\infty$ controller design software, together to form a software package IMC. If some information of the physical system (like pulse responses), or a mathematical model is available, the software will go through the whole integrated process automatically such that a person who has no knowledge of MATLAB can design controllers using this software. This software is programmed in MATLAB which is available in most workstations.

The main idea of this software is shown in Figure 1. For a physical system, the mathematical model of the given system can be obtained by identification or by mathematical modeling. Then the software starts either with the signals which are necessary for identification or with the given mathematical model. Based on the given model or identified model, the integrated process will produce controllers for evaluation. If the requirements of the evaluation are satisfied, the controllers can be implemented in the hardware equipment for testing.

For this experiment, we used the finite element model plus sensor and actuator dynamics as our evaluation model. The IMC controller design process is shown in Figure 2. The IMC software (Version imc_g03) has seven modules as follows.

i) Constructing a continuous and discrete evaluation model from the given finite element model.

ii) Constructing a design model by MCA model reduction.

iii) Constructing a discrete evaluation model by identification (not available).

iv) $\alpha$-loop study — discrete OVC controller design.

v) $\alpha$-loop study — discrete BOCC controller design.

vi) $\alpha$-loop study — discrete $EOL_\infty$ controller design.

vii) Evaluation Tool.

To design a controller from the finite element model, one can use modules i) and ii) to form the discrete state space evaluation and design models. Choosing an $\alpha$-loop controller design module, (for example, the BOCC $\alpha$-loop study), one can iterate on the modules ii) and iv) to carry on the Q-loop. After the Q-loop has converged, one can evaluate designed controllers using module vii). Now let us introduce each module in detail.

Using frequencies and mode shape vectors obtained from the finite element analysis, the first module combines the finite element model with sensor and actuator dynamics to form a continuous time state space model. By choosing a proper sampling rate, the discrete evaluation model can be obtained by discretizing the continuous time model. In the case that the order of the finite element model is relatively high, an additional (optional) MCA model reduction can be applied to obtain a lower order evaluation model.

The MCA model reduction module includes two kinds of MCA model reduction routines, continuous and discrete versions. The discrete reduced order model can be obtained from the discretized high order model by both continuous and discrete MCA model reductions, because both MCA results provide the contribution of each mode to the total cost, which can be used to decide which mode should remain in the design model. Also a modal cost analysis table will be generated.

Using the pulse responses or white noise responses, the identification module (not yet available) will produce an identified evaluation model by the q-Markov COVER method in [11-13].

The $\alpha$-loop study modules for the OVC, BOCC and $EOL_\infty$ controller design are similar. Here we only discuss the BOCC $\alpha$-loop study module. The block diagram of the BOCC $\alpha$-loop study is shown in Figure 2. The main philosophy of the $\alpha$-loop study is to obtain a sequence of the controllers from low control effort to high. As a result, the controller of the "best" performance can be obtained among those controllers.

The evaluation tool box module includes seven blocks described as follows.

i) Plotting pole locations.

ii) Discrete simulation of pulse responses.

iii) Plotting output variances with respect to $\alpha$.

iv) Simulation with arbitrary input functions.

v) Continuous simulation of pulse responses.

vi) Transferring MATLAB data file to ASCII code data files.

vii) Plotting FORTRAN simulation responses.

## 4. CONTROLLER DESIGN AND EXPERIMENTAL RESULTS

### 4.1 System Description and State Space Model

The JPL Large Space Control Laboratory Experiment Facility [14] is shown in the Figure 4. The main component of the apparatus consists of a central hub to which 12 ribs are attached. The diameter of the dish-like structure is slightly less than about 19 feet, the large size being necessary to achieve the low frequencies desired. The ribs are coupled together by two rings of wires which are maintained under nearly constant tension. Functionally, the wires provide coupling of motion in the circumferential direction which would otherwise occur only through the hub. The ribs, being quite flexible and unable to support their own weight without excessive droop, are each supported at two locations along their free length by levitators. A levitator assembly consists of a pulley, a counterweight, and a wire attached to the counterweight which passes over the pulley and attaches to the rib. The hub is mounted to the backup structure through a gimbal arrangement so that it is free to rotate about two perpendicular axes in the horizontal plane. A flexible boom is attached to the hub and hangs below it, and a weight, simulating the feed horn of an antenna, is attached at the bottom end of the boom. A 3 foot long boom is used for this experiment.

Actuation of the structure is as follows. Each rib can be individually manipulated by a rib-root actuator mounted on that rib near the hub. A rib root actuator reacts against a mount which is rigidly attached to the hub. In addition, two actuators are provided which torque the hub about its two gimbal axes. The hub torquers do not provide torque directly but rather are linear force actuators which produce torque by pushing or pulling at the outer circumference of the hub. The placement of these actuators guarantees good controllability of all of the flexible modes of motion. The locations of the actuators are shown in Figure 5. Two hub actuators are used for control in x and y directions. They are denoted by HA1 and HA10 respectively. The transfer

function from command torque to net torque is shown as follows.

$$\frac{T(s)}{T_c(s)} = \frac{3947.8}{s^2 + 44.43s + 3947.8} \quad . \tag{4.1}$$

Only four rib root actuators are used in this experiment. They are rib root actuators on ribs 1, 4, 7 and 10, denoted by RA1, RA4, RA7 and RA10. The transfer function from the command force to the net force is

$$\frac{F(s)}{F_c(s)} = \frac{24674}{s^2 + 111.1s + 24674} \quad . \tag{4.2}$$

The sensor locations are also shown in Figure 5. First, each of the 24 levitators is equipped with a sensor which measures the relative angle of the levitator pulley. The levitator sensors thus provide, in an indirect manner, the measurement of the vertical position of the corresponding ribs at the points where the levitators are attached. Four position sensors measure rib displacement at the rib-root actuator locations. Sensing for the hub consists of two rotation sensors which are mounted directly at the gimbal bearing. There are a total of 24 levitator sensors used for measurements. They are denoted by LS1 to LS24. The transfer function from the physical output to the measurement is assumed to be one because the optical sensor has pretty wide bandwidth. Two hub optical angle sensors, HS1 and HS10, are used to measure the hub angle in x and y directions. Similarly, the transfer function is assumed to be one. Only four rib root sensors, RS1, RS4, RS7 and RS10, are available for measurements. The dynamics are omitted (the transfer function is assumed to be one). Since the hub and rib root sensors are very noisy, a first order filter is applied for each of those six sensors. The transfer function of the filter is

$$H(s) = \frac{502.65}{s + 502.65} \quad . \tag{4.3}$$

A summary of outputs and inputs is contained in Table 1.

JPL created two finite element models with 30 and 84 modes respectively. The 30 mode finite element model is used in this experiment. All modes with natural frequencies less than 10 Hz are given in Table 2. Let the structure be described in its modal coordinates by the following

$$\left.\begin{aligned} \ddot{\eta}_i + 2\xi_i\omega_i\dot{\eta}_i + \omega_i^2\eta_i &= b_i^T u_a \ , \ i = 1, 2, ..., 30 \\ y &= \sum_{i=1}^{30} p_i\eta_i \end{aligned}\right\} , \tag{4.4}$$

where $u_a$ is the actuator output signal and y is the displacement vector co-located with the sensor inputs. JPL provided 30 frequencies ($\omega_i$, i = 1, 2, ..., 30) and 30 mode shapes ($p_i$, i = 1, 2, ..., 30) obtained from a finite element analysis.

The actuator output signal $u_a$ is now filtered by hub actuator and rib root actuator dynamics modeled by the following

$$\left.\begin{aligned} \dot{x}_a &= A_a x_a + B_a u \\ u_a &= C_a x_a + w_p \end{aligned}\right\} , \tag{4.5}$$

where u is composed of the command signals to the hub and rib root actuators, and $w_p$ is the actuator noise with intensity $\overline{W}_p$. The measurement output z now can be presented by

$$\left.\begin{aligned} \dot{x}_s &= A_s x_s + B_s y \\ z &= C_s x_s + D_s y + v \end{aligned}\right\} , \tag{4.6}$$

where v is the sensor noise with intensity $\overline{V}$. Combining models (4.4-4.6), we can obtain a continuous time full order model. Since the frequencies of all modes in our model are less than 5 Hz, we discretize the continuous model at 25 Hz which is the computer sample rate. The discrete *evaluation model* is as follows.

$$\left.\begin{aligned} x_e(k+1) &= A_e x_e(k) + B_e u(k) + D_e w_p(k) \\ y_p(k) &= C_e x_e(k) \\ z(k) &= M_e x_e(k) + v(k) \end{aligned}\right\} , \tag{4.7}$$

where $w_p$ and v are white noise with covariance matrix $W_p = \overline{W}_p/25$ and $V = \overline{V}/25$ respectively.

## 4.2 The BOCC Controller Design and Experimental Results

The design strategy used here is the integration of model reduction and controller design introduced in the last section. Using the open loop experimental results at JPL, we adjusted some frequencies, damping coefficients and input/output magnitudes such that the responses of the finite element model combining with the sensor and actuator dynamics were closer to the experimental pulse responses. The adjusted frequencies and damping coefficients are shown in Table 2. The magnitude coefficients vary in different designs.

### 4.2.1 The OVC Design and Experimental Results

#### The OVC Controller Design

We start controller design with the OVC algorithm because the OVC problem is a special case of the BOCC. Note that in this case the constraints on the output covariance matrices reduce to those on output variances. Hence, all the constraints are scalars. Some errors in the finite element model of the structure are found. The errors result from the sign convention on the hub sensors. Also the units used in the finite element model and those used in the real-time control computer are different. The units used in the measurement and output are meter and radian in the finite element model but those in real-time control computer are milli-meter and milli-radian. We use input/output scaling matrices to overcome unit differences and finite element modeling errors. The input scaling matrix is

$$S_u = \text{diag}[0.5, -1, 1, 1, 1, 1]e{+}3 \ , \tag{4.8}$$

and the output scaling matrix $S_y$ is a diagonal matrix with unity diagonal entries except the 26th diagonal element which is negative unity. The finite element model provided by JPL is modified by redefining the input vector $S_u u_a$ and output vector $S_y y$ as $u_a$ and y in (4.4) respectively. The evaluation model used in this design is obtained by combining the modified finite element model, sensor and actuator dynamics in (4.4-4.6). The evaluation model is discretized at a sampling frequency 25 Hz. The state space realization of this model is in the form (4.7), where $A_e$, $B_e$, $D_e$, $C_e$ and $M_e$ are the system matrices respectively of dimension $78 \times 78$, $78 \times 6$, $78 \times 6$, $30 \times 78$ and $30 \times 78$, and u, $y_p$ and z are input, output and measurement vectors, respectively, as described in Table 1. Vector $w_p$ is the system noise from hub and rib root actuators with the following variances,

$$W_p = \text{diag}[0.04,\ 0.04,\ 0.04,\ 0.04,\ 0.04,\ 0.04] \ . \qquad (4.9)$$

Vector v is the measurement noise of the levitator, hub and rib root sensors with the following variance,

$$V = \text{block diag}\ [1.5625I_{22},\ 3.0500I_2,\ 0.2500I_4] \ , \qquad (4.10)$$

where the suffix of matrix I indicates the dimension of the identity matrix. All the variances are taken from signal to noise ratios.

In order to decide the order of the controller to be used, we designed 12th, 16th, 20th and 24th order controllers for the first Q-loop. It turns out that 16th, 20th and 24th order controllers have close performances with respect to the evaluation model. But the 12th order controller yields poor performance. Hence, we choose controller order to be 16. The 16th order controller is designed by using the design methodology presented in the last section.

The design parameters used in this design for the Q–loop are

$$\beta = 0.2 \ ; \ \alpha_q = 0.5 \ ; \ \alpha_w = 0.5 \ . \qquad (4.11)$$

We compute the open loop output variance $Y_i(0)$ with respect to the evaluation model, and the lower bound $L_i$ for the design model.

The Modal Cost Analysis results for the different Q–loops 1 and 3 can be found in Table 3. The first 8 dominant modes in the Q-loop 1 and 3 are the same. Hence, in this case the Q-loop will not converge but oscillate between two models which are obtained in Q-loop 1 and 2. Since the "best" performance with respect to the evaluation model is obtained in Q-loop 2, we use the reduced order model of Q-loop 2 which keeps modes 2, 1, 14, 13, 27, 28, 4 and 6 as the final design model. The iteration on the Q-loop is terminated at Q-loop 3.

Note that for each Q-loop the OVC $\alpha$-loop algorithm produces a number of controllers from low to high control effort. The input/output variance curves of Q-loop 2 for the 16th order controller design are shown in Figure 6. The solid curve with "o" is the performance of the controllers obtained from the OVC algorithm evaluated with the design model. The dashed line with "*" evaluates these controllers with the evaluation model. In the $\alpha$-loop study, 13 controllers are produced. The first 12 controllers stabilize the evaluation model. The output variances of the closed loop system with respect to the evaluation model are plotted in Figure 6. The $\alpha$-loop iterations terminate because the 13th controller destabilizes the evaluation model.

From Figure 6 it can be observed that the "best" performance for outputs 4 and 5 is provided by the closed loop systems obtained by evaluating controllers 8 and 9 with the evaluation model. Similar input/output variance curves of Q-loop 0 are obtained. In order to show the improvement of iterating the design model, we compute the differences between the output variances of Q-loop 0 and those of Q-loop 2 for each output. Let $Y_2(i,j)$ and $Y_0(i,j)$ denote the ith output variance obtained by evaluating the jth controllers of Q-loop 2 and 0 with the evaluation model respectively. Plots $[Y_2(i,8) - Y_0(i,8)]/Y_0(i,8)$ and $[Y_2(i,9) - Y_0(i,9)]/Y_0(i,9)$ can be found in Figure 7. Since plots for controllers 8 and 9 are negative for almost all outputs, it is clear that the Q-loop improves the model reduction and controller design process, i.e., a better controller with respect to the evaluation model can be obtained by integration of model reduction and controller design.

## The OVC Controller Experiment

Controllers 1, 3, 5, 7, 9, 11 and 13 of Q-loop 2 were tested on the JPL LSCL Experiment Facility. It is expected that the responses of controller 1 are pretty close to the open loop ones due to low control effort. The sequence of controllers allows one to do lab tests easily with little risk of damaging the system. Starting with low control effort controller, we can test controllers one by one with increased control effort, and stop the test when some controller destabilizes the system, or the oscillations become unacceptable. Because the control effort is increased gradually, the test facility will not be damaged. This is a nice feature of the integrated controller design strategy.

Since the system is highly damped, a pulse input with the width equal to a sample period (0.04 second) does not excite the system much. Hence, it is difficult to compute all the output variances by experimental data. We did the pulse experiments for each controller obtained in Q-loop 2 with pulse input on HA1 and HA10 respectively, where the magnitude of the pulse is 2 Newton-meters, and the width is 4 seconds (100 sample periods). We computed the input and output $\ell_2$ norms in the following way

$$\|u(\cdot)\|_2^2 \triangleq \Delta^2 \sum_{k=101}^{p} u^T(k)u(k) \; ; \tag{4.12a}$$

$$\|y_i(\cdot)\|_2^2 \triangleq \Delta^2 \sum_{k=101}^{p} y_i^2(k) \; , \tag{4.12b}$$

where $\Delta = 0.04$ second is the sample period and $p = 1001$ is the number of sample

periods used for the test. Using (4.12) Figure 8 presents plots of input/output $\ell_2$ norms for outputs 4, 5, 16 and 17, where the dotted line with "+" is associated with experimental data, dashed line with "*" is obtained from simulated data with the evaluation model, and the solid line with "o" is also from simulated data but with the design model. Note that we did not test every controller designed in the $\alpha$-loop study of Q-loop 2. Hence, the "+" signs on Figure 5.4 are the $\ell_2$ norms of the open loop responses and closed loop responses related to controllers 1, 3, 5, 7, 9, 11 and 13 from left to right. Due to noisy data and the difference between the finite element model and the real structure, lab tested $\ell_2$ norm curves stay above the simulated ones. It is obvious that the 9th controller in the $\alpha$-loop study of Q-loop 2 provides the "best" closed loop $\ell_2$ response, which is consistent to the $\alpha$-loop study result. In the $\alpha$-loop study of Q-loop 2, the 13th controller destabilizes the evaluation model. It turns out that the closed loop system with that controller is unstable, too. It is clear from Figure 8 that the $\ell_2$ norms blow up for controller 13. Hence, the test result agrees with the analytic one. The controller yielding the best performance experimentally is the best controller from the analytical designs.

Because the control experiment facility has no special channels to apply disturbances, the test has been done in such a way that the system is open loop at $t = 0$, when exciting signals are applied to the structure through control actuators. When the open loop command signals vanish, the control loop will be closed to conduct the closed loop experiment. Hence, the exciting signals applied through the actuator channels provide the initial condition for the structure.

The pulse responses of HA1 with controller 9 of Q-loop 2 are shown in Figure 9, where all input pulses are with the magnitude 2 Newton-meters and period 4 seconds. Hence, the closed loop control started at the 4th second, and open and closed loop responses are supposed to be the same for the first 4 seconds. It is obvious that the first two modes with frequency 0.0902 Hz are excited. From those responses, it is clear that the controller improves the performance of the system.

### 4.2.2 The BOCC Design and Experimental Results

The BOCC Controller Design

From the experience of the OVC controller design we feel that it is not necessary to use all outputs for controller design because of the symmetrical property of the structure. Hence, we choose to reduce the output number for the model reduction and control design process but still use all 30 measurements for the control design purpose. Outputs used for the BOCC design are

$$y_p = [y_1\ y_4\ y_{13}\ y_{16}\ y_{25}\ y_{26}\ y_{27}\ y_{28}]^T \ . \tag{4.13}$$

We group outputs in the following way

$$\hat{y}_1 \triangleq \begin{bmatrix} y_1 \\ y_4 \end{bmatrix} \ ; \ \hat{y}_2 \triangleq \begin{bmatrix} y_{13} \\ y_{16} \end{bmatrix} \ ; \ \hat{y}_3 \triangleq \begin{bmatrix} y_{25} \\ y_{26} \end{bmatrix} \ ; \ \hat{y}_4 \triangleq \begin{bmatrix} y_{27} \\ y_{28} \end{bmatrix} \ . \tag{4.14}$$

Hence, in this case constraints of the BOCC problem are $2 \times 2$ matrices for all output groups. Physical interpretation of this design is clear. Consider the output group $\hat{y}_3$ which is hub angle in x and y directions. Suppose that the maximal singular value of the constraint matrix is $\sigma_3$. Then the design will guarantee that the hub angle at any direction of x–y plane will be less than or equal to the square root of $\sigma_3$ times the input $\ell_2$ norm.

According to the lab test of the OVC controllers, the output scaling matrix is changed as follows

$$S_y = \text{block diag}[I_{24},\ 1,\ -1,\ 0.1I_4] \ , \tag{4.15}$$

where the subscript of matrix I denotes the dimension of the identity matrix. The input scaling matrix remains unchanged.

The noise covariance matrix $W_p$ is changed to a non-diagonal one to allow correlated noise on rib root actuators, where

$$W_p = \begin{bmatrix} 0.040 & 0.000 & 0.000 & 0.000 & 0.000 & 0.000 \\ 0.000 & 0.040 & 0.000 & 0.000 & 0.000 & 0.000 \\ 0.000 & 0.000 & 0.720 & 0.360 & 0.360 & 0.360 \\ 0.000 & 0.000 & 0.360 & 0.720 & 0.360 & 0.360 \\ 0.000 & 0.000 & 0.360 & 0.360 & 0.720 & 0.360 \\ 0.000 & 0.000 & 0.360 & 0.360 & 0.360 & 0.720 \end{bmatrix} . \quad (4.16)$$

We choose to design the 20th order controller for the BOCC problem. The design parameters used in this design for the Q-loop are

$$\beta = 0.2 \ ; \ \alpha_q = 0.5 \ ; \ \alpha_r = 0.5 \ . \quad (4.17)$$

The open loop output covariance matrix and lower bound of the output covariance matrix are computed in same way as in the OVC design.

The MCA model reduction results of the BOCC design is quite similar to the OVC Case. The Q-loop does not converge but oscillates between two design models. We plot the closed loop output maximal singular value curves with respect to the summation of input variances, where the maximal singular values are computed with respect to the design and evaluation models. The plot for Q-loop 2 is shown in Figure 10, where all symbols have the same meaning as those in the OVC design. It is observed that the "best" performance of output group 1, which is difficult to be achieved by the design, is provided by the 12th controller designed in Q-loop 2. Those controllers designed in Q-loop 2 were tested in the lab. In the $\alpha$-loop, fifteen controllers are designed. All controllers stabilize the evaluation model. The 12th controller provides the "best" performance for output group 2.

## The BOCC controller Experiment

The controllers 1, 3, 5, 7, 9, 11 and 13 of Q-loop 2 were tested on the JPL LSCL Experiment Facility. We define the $\ell_2$ norm for each output group as

$$\|\hat{y}_i(\cdot)\|_2^2 \triangleq \Delta^2 \sum_{k=101}^{P} \hat{y}_i^T(k)\hat{y}_i(k) \ ; \ i = 1, 2, ..., 4 \ , \quad (4.18)$$

with the same definition on the input $\ell_2$ norm as in the OVC case. The input/output $\ell_2$ norm curves of the BOCC test are shown in Figure 11. From the input/output $\ell_2$ norm plots in Figure 5.11, the "best" $\ell_2$ performances are obtained by the 11th controller of Q-loop 2. The analytical $\ell_2$ responses of output group 4 are quite different from the

test. We have no definitive answer, but we attribute such difference to nonlinearity and friction. All experiments have been done in the same way as the OVC design. The pulse responses of controller 11 with the same exciting signals as the OVC test can be found in Figure 12.

## 5. CONCLUSIONS

A reduced order controller design methodology with an integration of model reduction and controller design has been applied to the JPL LSCL Experiment Facility. This design strategy is an extension of that in [10,15]. The design strategy has provided a practical method for large space structure controller synthesis. The application of this strategy to the JPL LSCL Experiment Facility has met our high expectation.

From this experiment, we see that iterating between modeling and control (selecting an "appropriate" design model) plays an important role in the controller design. For two different design objectives (the OVC and BOCC designs), the iteration in the Q-loop improves the design model, which indicates that the integration of model reduction and controller design does improve the controller synthesis.

This is the first BOCC controller design tested in lab. The BOCC design algorithm, which is a generalization of the OVC and OCC algorithms, works well for this project. The difference in the performance between the OVC and BOCC design is attributed to the difference in the type of design specifications, rather than any preference for one method over the other. The BOCC is much more general, including the OVC as a special case.

Finally, a MATLAB software package IMC has been produced to integrate modeling and controller design for flexible structures. This is the first experimental test of this software.

## 6. LIST OF REFERENCES

[1] G. Zhu and R.E. Skelton, "Mixed $\mathcal{L}_2$ and $\mathcal{L}_\infty$ problems by weight selection in quadratic optimal control," *Int. J. Control, Vol. 53, No. 5, 1991.*

[2] C. Hsieh and R.E. Skelton, "Minimum energy controllers satisfying inequality output variance constraints," *Appl. Methods, Vol. 10, No. 4, 347-366, 1989.*

[3] G. Zhu and R. E. Skelton, "Controller Design to Achieve Covariance Constraints," *IFAC Symposium on Design Methods of Control System, Zurich, Switzerland, Sep., 1991.*

[4] G. Zhu, "$\mathcal{L}_2$ and $\mathcal{L}_\infty$ Multiobjective Control for Linear Systems," *PhD Dissertation, Purdue University, May, 1992.*

[5] G. Zhu and R. E. Skelton, "A Two-Riccati Feasible Algorithm for Guaranteeing Output $\mathcal{L}_\infty$ Constraints," *Proceedings of Control and Decision Conference, 1991.*

[6] R. E. Skelton, *Dynamics System Control*, Wiley, New York, 1988.

[7] R. E. Skelton, R. Singh and J. Ramakrishnan, "Component Model Reduction by Component Cost Analysis," *Proc. AIAA Guid. and Contr. Conf., Minneapolis, MN, 1988.*

[8] J. H. Kim and R. E. Skelton, "Model Reduction by Weighted Component Cost Analysis," *AIAA Dynamics Specialists Conf., Long Beach, CA, 1990.*

[9] R. E. Skelton, P. C. Hughes and H. B. Hablani, "Order Reduction for Models of Space Structure Using Modal Cost Analysis," *J. Guid., Contr. and Dyn., Vol. 5, No. 4, 1982.*

[10] C. Hsieh, J. H. Kim, G. Zhu, K. Liu and R.E. Skelton, "An iterative algorithm combining model reduction and control design," *Proceedings of American Control Conference, pp 2120-2125, 1990.*

[11] R. E. Skelton and B. D. O. Anderson, "Q-Markov Covariance Equivalent Realization," *Int. J. Contr., Vol. 44, No. 5, 1986.*

[12] D. A. Wagie and R. E. Skelton, "A Projection Approach to Covariance Equivalent Realizations of Discrete Systems," *IEEE Trans. Auto. Contr., AC-31, 1986.*

[13] R. E. Skelton and E. G. Collins, "Set of Q-Markov Covariance Equivalent Model of Discrete Systems," *Int. J. Contr., Vol. 46, No. 1, 1987.*

[14] H. C. Vivian, P. E. Blaire, D. B. Eldred, G. E. Fleischer, C.-H. C.Ih, N. M. Nerheim, R. E. Scheid and J. T. Wen, "Flexible Structure Control Laboratory Development Technology Demonstration," *Jet Propulsion Laboratory, California Institute of Technology, 1987.*

[15] C. Hsieh, J. H. Kim and R. E. Skelton, "NASA GI Project-Purdue Annual Report," *NASA GI Project Annual Report Meeting, Hampton, VA, Jan., 1990.*

Table 1 Inputs, Outputs and Their Limits

| Inputs | | Outputs | |
|---|---|---|---|
| Hub Actuator | | Hub Sensor | |
| Notation | Limit | Notation | Limit |
| HA10 ($u_1$) | 2 (N-M) | HS1 ($y_{25}$) | 69.8 (mrad) |
| HA1 ($u_2$) | 2 (N-M) | HS10 ($y_{26}$) | 69.8 (mrad) |
| Rib Root Actuator | | Rib Root Sensor | |
| Notation | Limit | Notation | Limit |
| RA1 ($u_3$) | 2 (N) | RS1 ($y_{27}$) | 10 (mm) |
| RA4 ($u_4$) | 2 (N) | RS4 ($y_{28}$) | 10 (mm) |
| RA7 ($u_5$) | 2 (N) | RS7 ($y_{29}$) | 10 (mm) |
| RA10 ($u_6$) | 2 (N) | RS10 ($y_{30}$) | 10 (mm) |
| | | Levitator Sensor | |
| | | Notation | Limit |
| | | LS1–LS24 ($y_1 - y_{24}$) | 114.3 (mm) |

Table 2 Frequencies and Damping Coefficients

| Mode No. | Frequency (Hz) | | Damping Coeff. | |
|---|---|---|---|---|
| | (Original) | (Modified) | (Original) | (Modified) |
| 1 | 0.0902 | 0.0975 | 0.0100 | 0.1225 |
| 2 | 0.0902 | 0.0917 | 0.0100 | 0.2500 |
| 3 | 0.2089 | 0.2089 | 0.0263 | 0.0263 |
| 4 | 0.2527 | 0.2527 | 0.0100 | 0.0100 |
| 5 | 0.2527 | 0.2527 | 0.0100 | 0.0100 |
| 6 | 0.2894 | 0.2894 | 0.0100 | 0.0100 |
| 7 | 0.2894 | 0.2894 | 0.0100 | 0.0100 |
| 8 | 0.3218 | 0.3218 | 0.0100 | 0.0100 |
| 9 | 0.3218 | 0.3218 | 0.0100 | 0.0100 |
| 10 | 0.3435 | 0.3435 | 0.0100 | 0.0100 |
| 11 | 0.3435 | 0.3435 | 0.0100 | 0.0100 |
| 12 | 0.3509 | 0.3509 | 0.0100 | 0.0100 |
| 13 | 0.6150 | 0.6250 | 0.0200 | 0.0200 |
| 14 | 0.6150 | 0.6200 | 0.0300 | 0.0300 |
| 15 | 1.5083 | 1.5083 | 0.0100 | 0.0100 |
| 16 | 1.5295 | 1.5295 | 0.0100 | 0.0100 |
| 17 | 1.5295 | 1.5295 | 0.0100 | 0.0100 |
| 18 | 1.5461 | 1.5461 | 0.0100 | 0.0100 |
| 19 | 1.5461 | 1.5461 | 0.0100 | 0.0100 |
| 20 | 1.5625 | 1.5625 | 0.0100 | 0.0100 |
| 21 | 1.5625 | 1.5625 | 0.0100 | 0.0100 |
| 22 | 1.5744 | 1.5744 | 0.0100 | 0.0100 |
| 23 | 1.5744 | 1.5744 | 0.0100 | 0.0100 |
| 24 | 1.5746 | 1.5746 | 0.0100 | 0.0100 |
| 25 | 1.6842 | 1.6842 | 0.0100 | 0.0100 |
| 26 | 1.6842 | 1.6842 | 0.0100 | 0.0100 |
| 27 | 2.5771 | 2.5771 | 0.0100 | 0.0100 |
| 28 | 2.5771 | 2.5771 | 0.0100 | 0.0100 |
| 29 | 4.8576 | 4.8576 | 0.0100 | 0.0100 |
| 30 | 4.8576 | 4.8576 | 0.0100 | 0.0100 |

Table 3 Modal Cost Analysis of the OVC design for Q-loop 1 and 3

| Index | Q-loop 1 | | Q-loop 3 | |
|---|---|---|---|---|
| | $\alpha_b = 9$ | | $\alpha_b = 9$ | |
| | Modal Cost | Mode No. | Modal Cost | Mode No. |
| 1 | 6.6723e+1 | 2 | 6.7071e+1 | 2 |
| 2 | 2.5040e+1 | 1 | 2.3619e+1 | 1 |
| 3 | 4.2676e+0 | 14 | 4.8554e+0 | 14 |
| 4 | 2.2173e+0 | 13 | 2.6104e+0 | 13 |
| 5 | 4.7986e-1 | 4 | 4.7182e-1 | 4 |
| 6 | 2.0138e-1 | 8 | 1.9765e-1 | 8 |
| 7 | 1.9129e-1 | 3 | 1.8981e-1 | 7 |
| 8 | 1.7050e-1 | 7 | 1.7689e-1 | 3 |
| 9 | 1.4221e-1 | 6 | 9.9888e-2 | 6 |
| 10 | 8.7302e-2 | 11 | 7.9285e-2 | 16 |
| 11 | 7.9527e-2 | 12 | 7.8692e-2 | 11 |
| 12 | 7.8317e-2 | 10 | 7.5395e-2 | 10 |
| 13 | 5.2735e-2 | 16 | 7.3416e-2 | 20 |
| 14 | 4.8844e-2 | 20 | 7.3290e-2 | 12 |
| 15 | 3.3937e-2 | 27 | 5.8980e-2 | 28 |
| 16 | 3.2116e-2 | 28 | 4.9655e-2 | 27 |
| 17 | 2.6763e-2 | 15 | 3.8368e-2 | 19 |
| 18 | 2.5116e-2 | 19 | 3.8337e-2 | 15 |
| 19 | 2.3742e-2 | 24 | 3.4985e-2 | 23 |
| 20 | 2.3351e-2 | 23 | 3.4597e-2 | 24 |

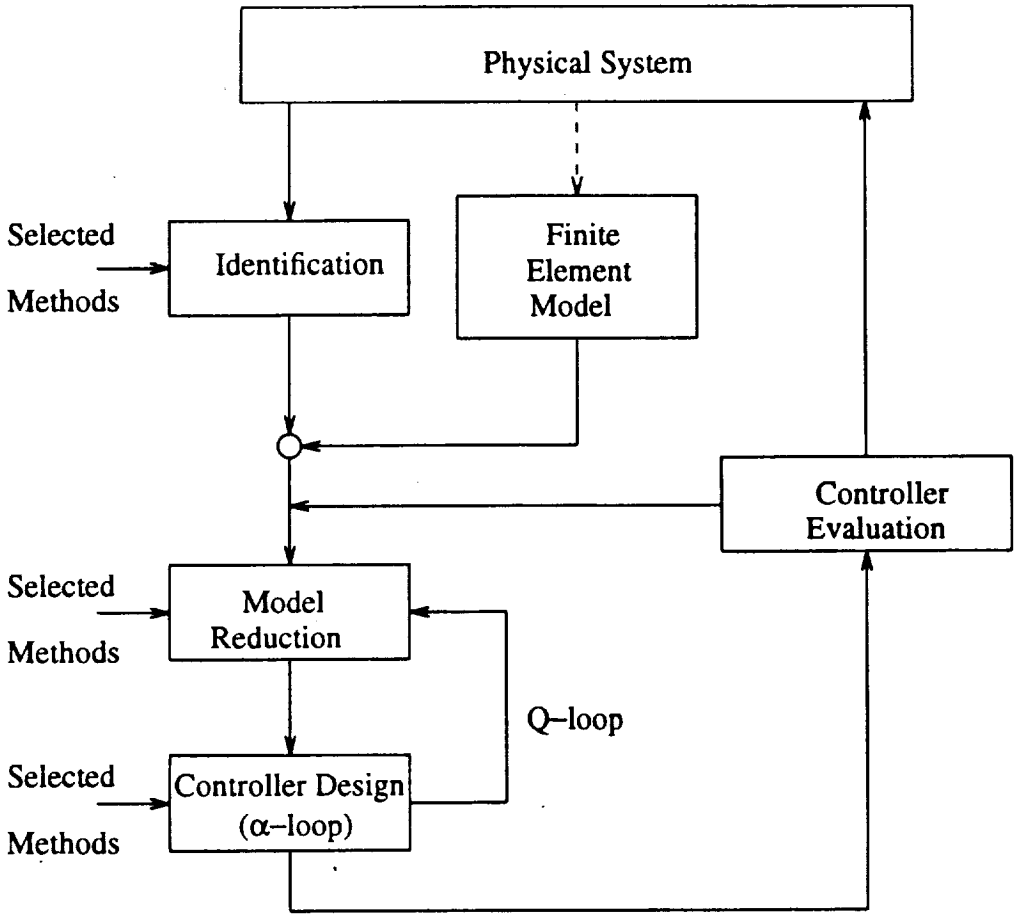


Figure 1 Flowchart of the IMC Software

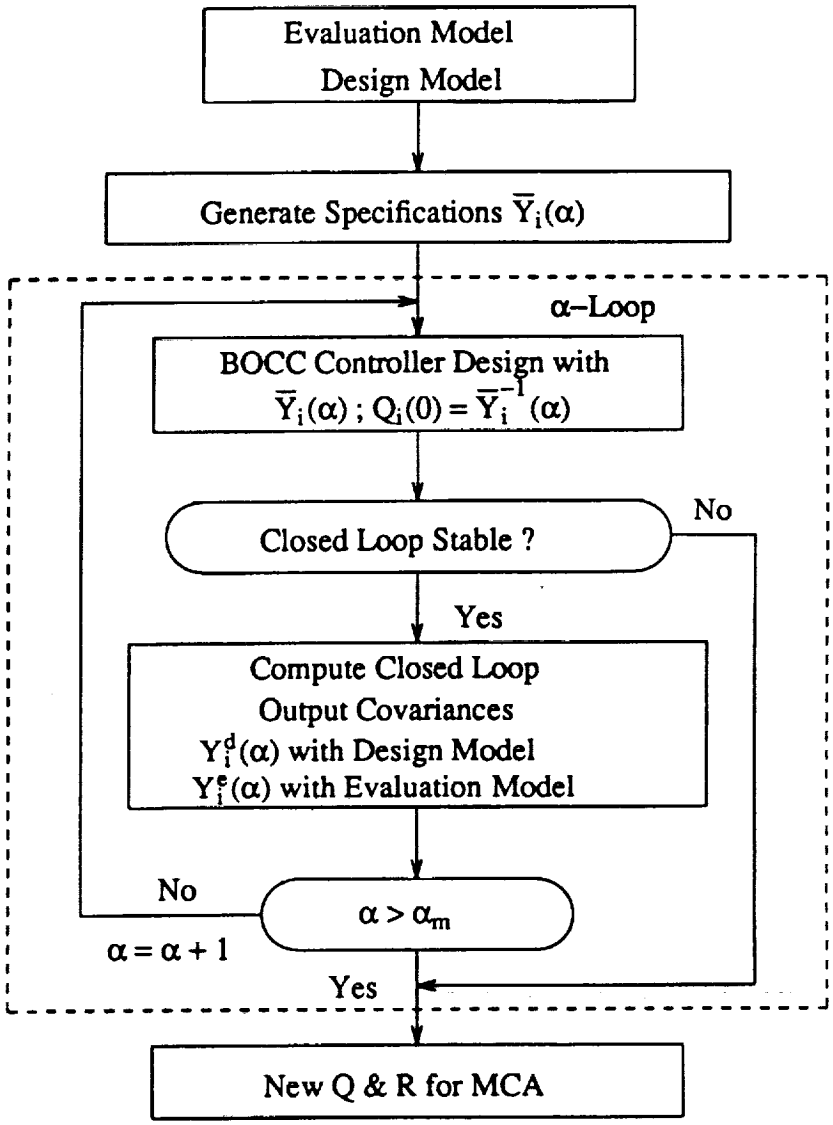


Figure 2 The BOCC α-loop Study

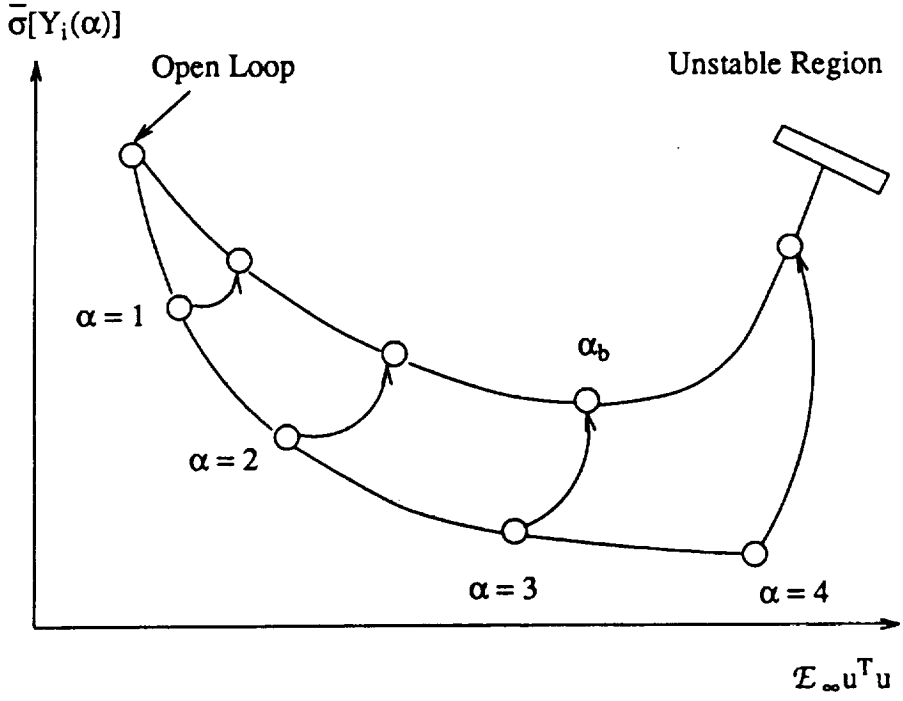


Figure 3 Tradeoff of Output Covariance and Input Variances

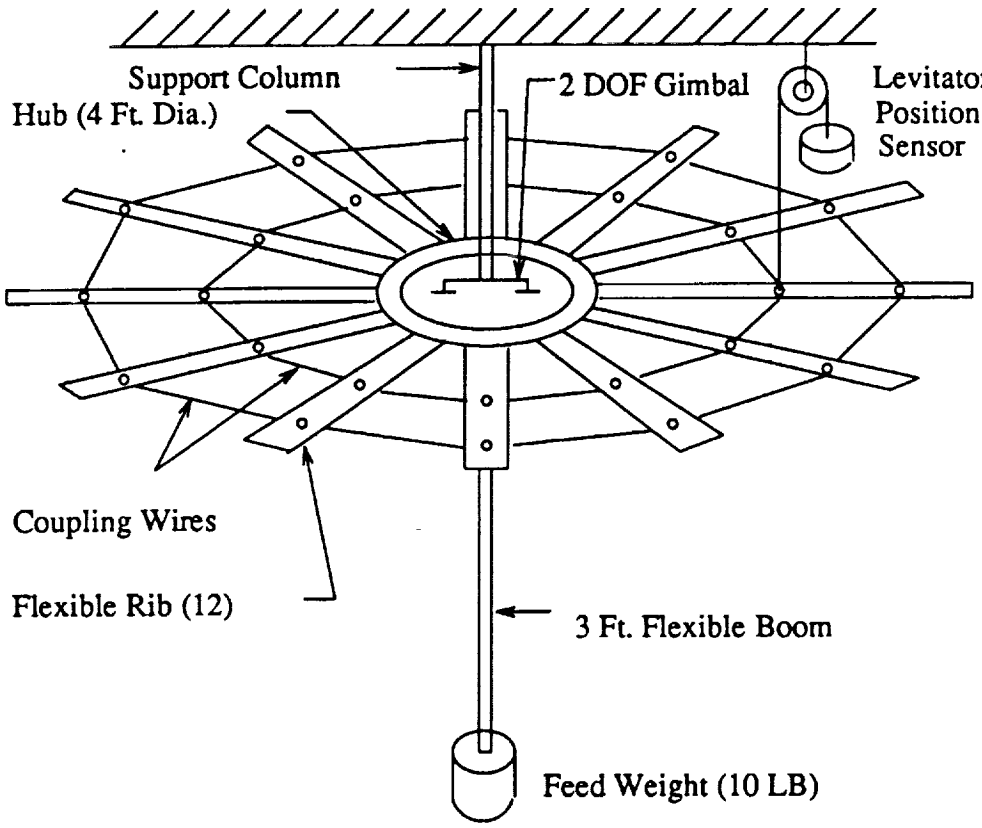


Figure 4 Experiment Structure

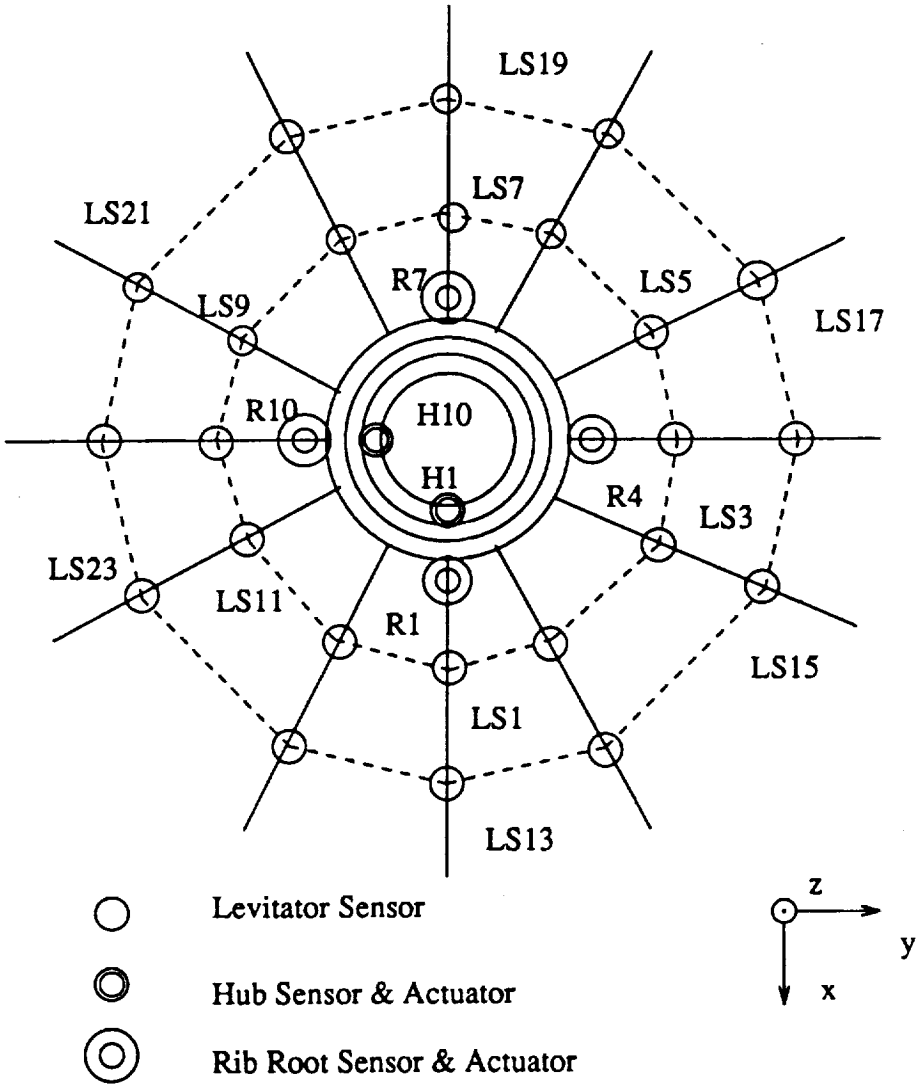


Figure 5 Transducer Locations and Labeling

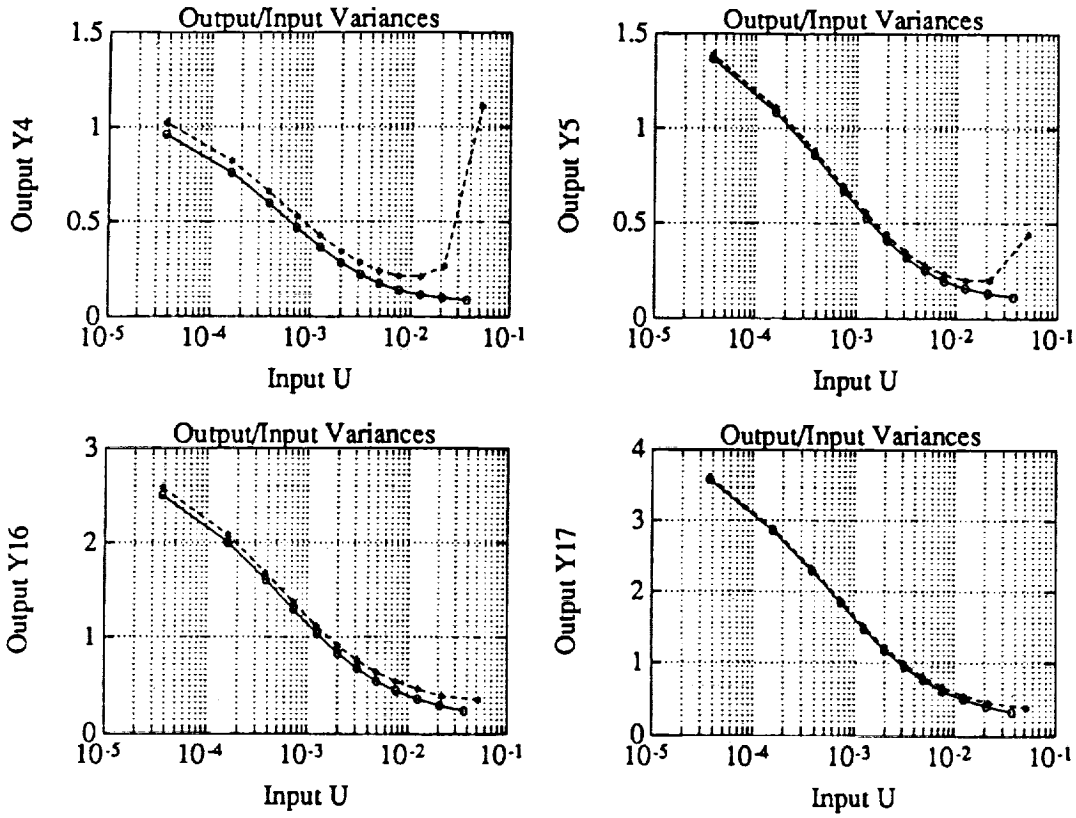


Figure 6 Input/Output Variance Curves for the OVC Design

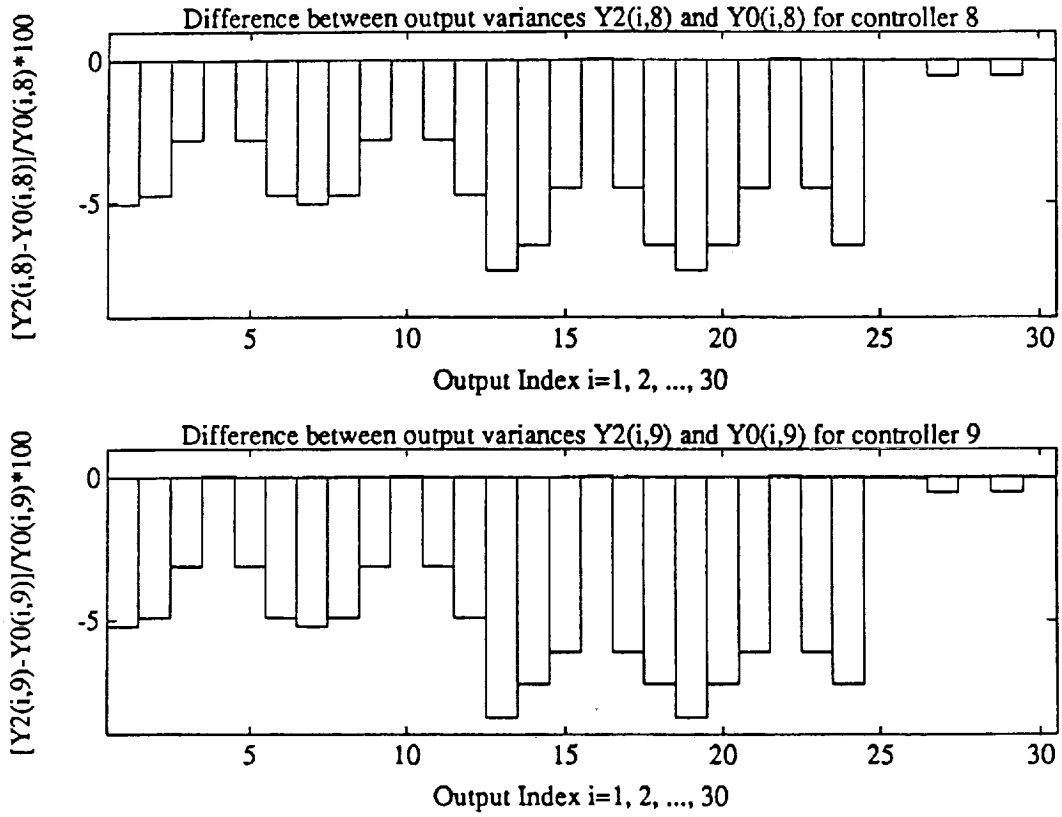


Figure 7 Output Variance Differences of Q-loop 0 and 2

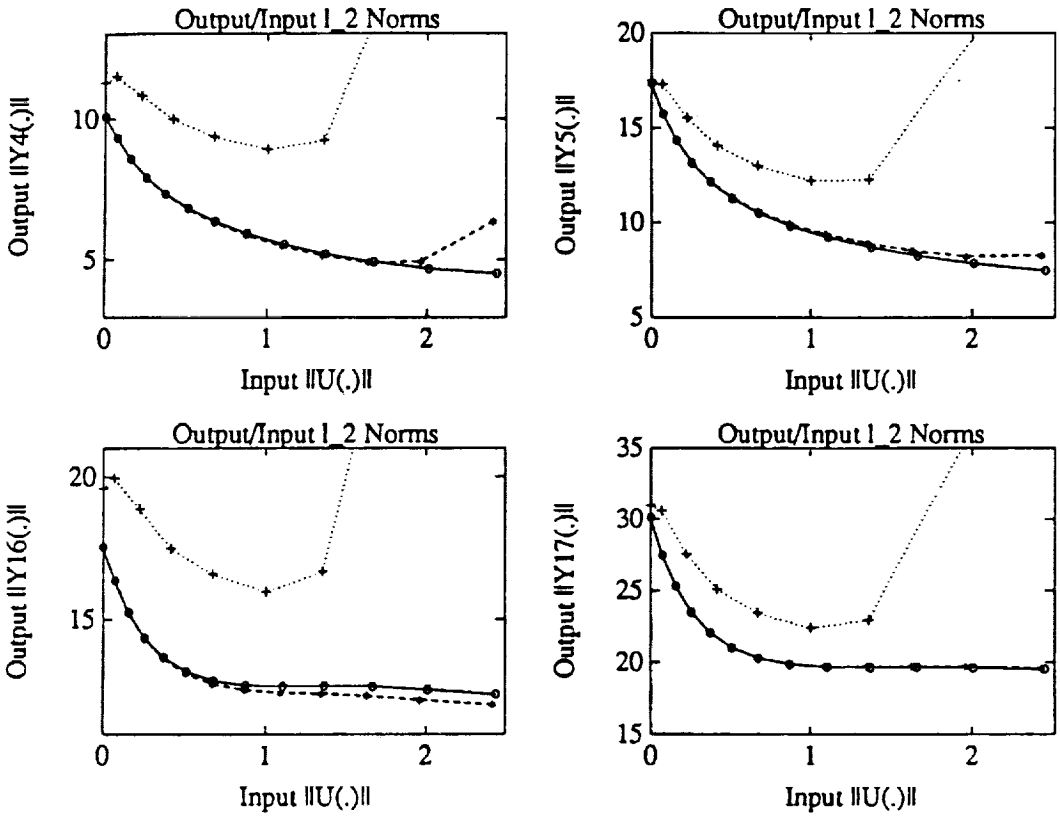


Figure 8 Input/Output $\ell_2$ Norm Curves for the OVC Design

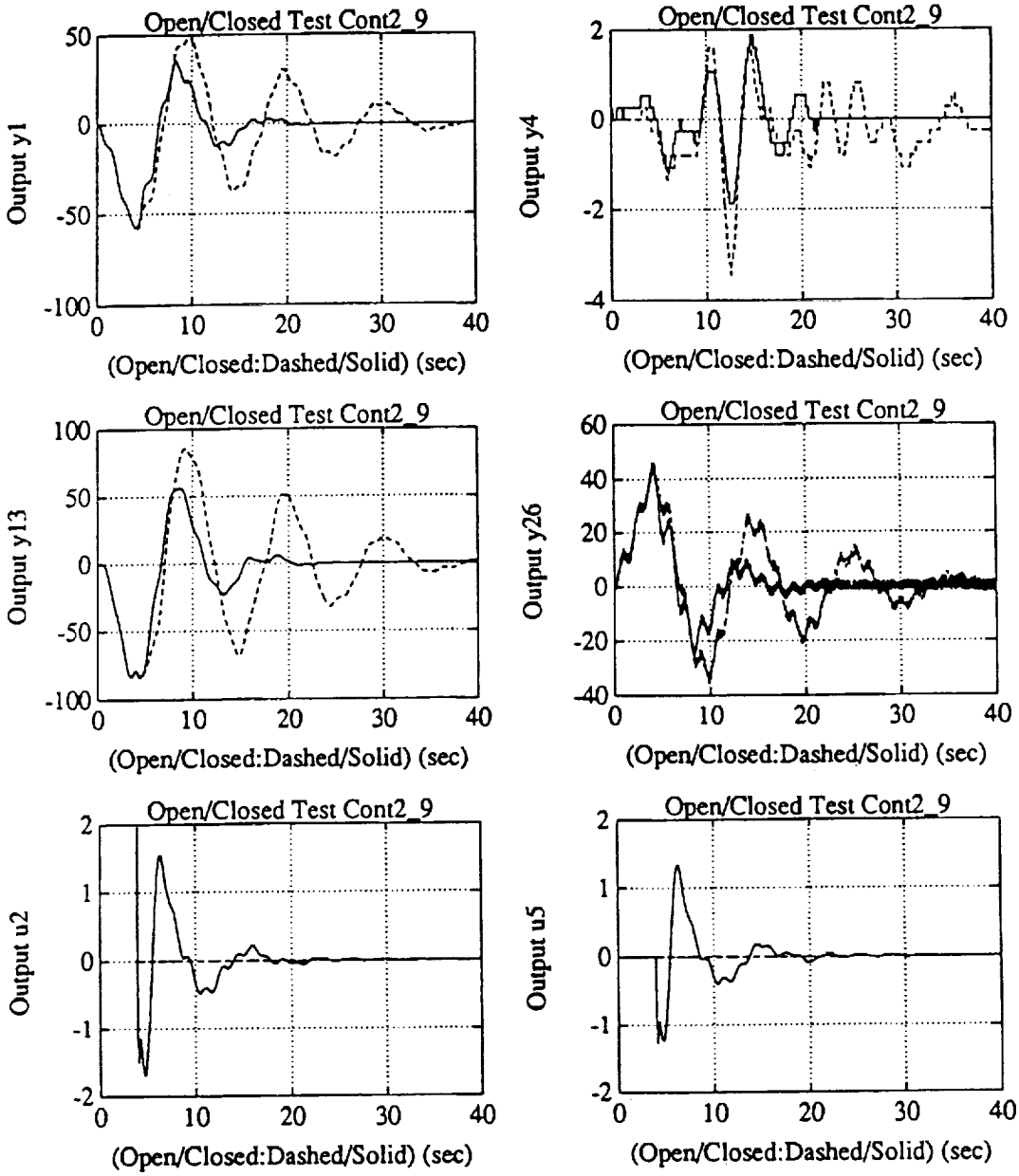


Figure 9 Y Direction Pulse Responses of the OVC Design

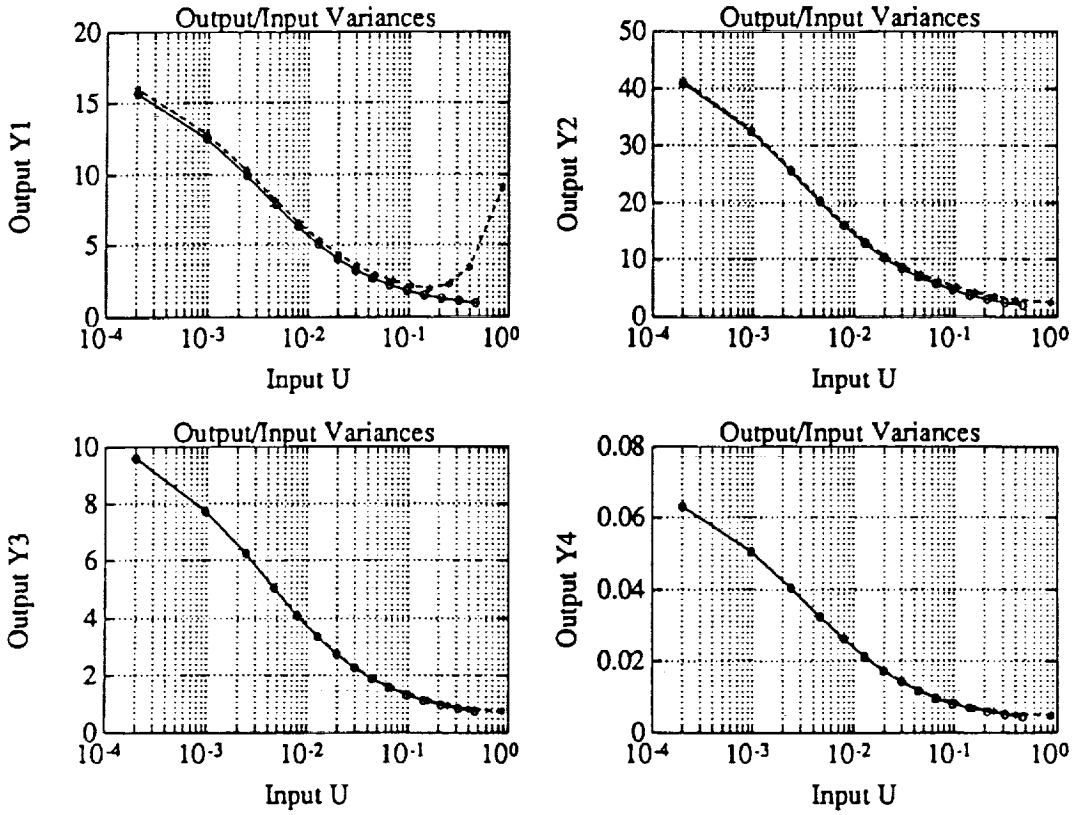


Figure 10 Input/Output Variance Curves for the BOCC Design

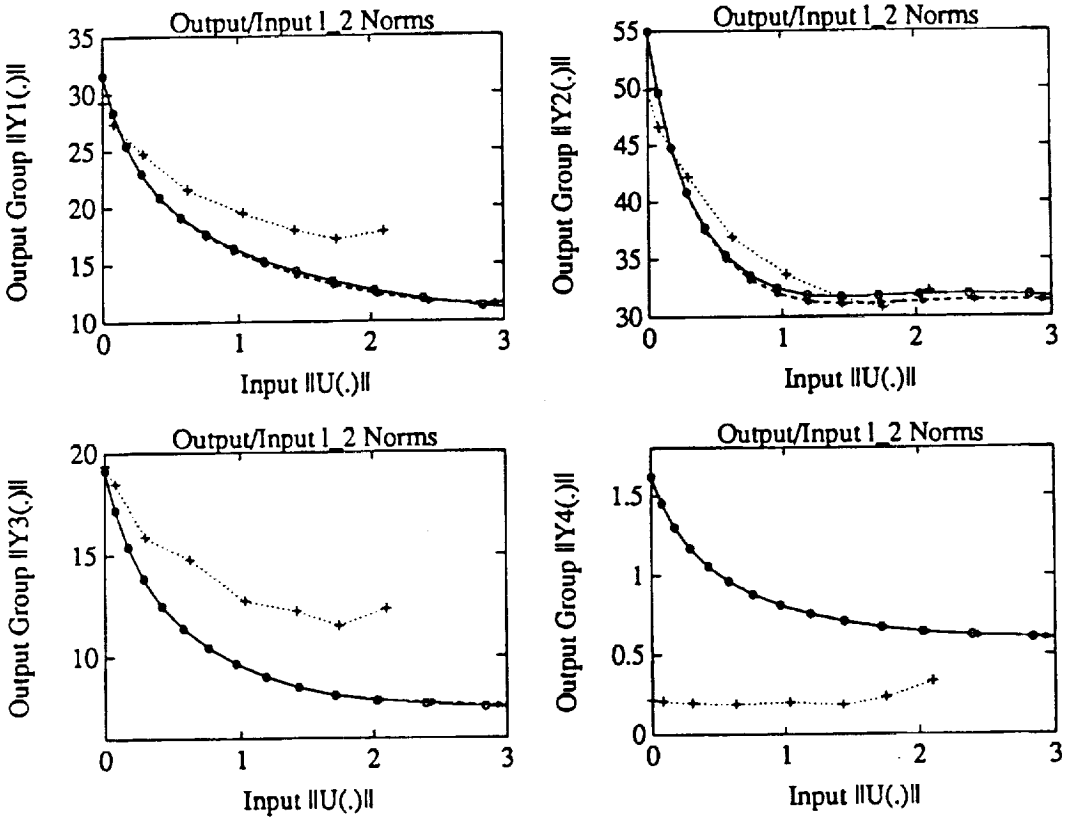


Figure 11 Input/Output $\ell_2$ Norm Curves for the BOCC Design

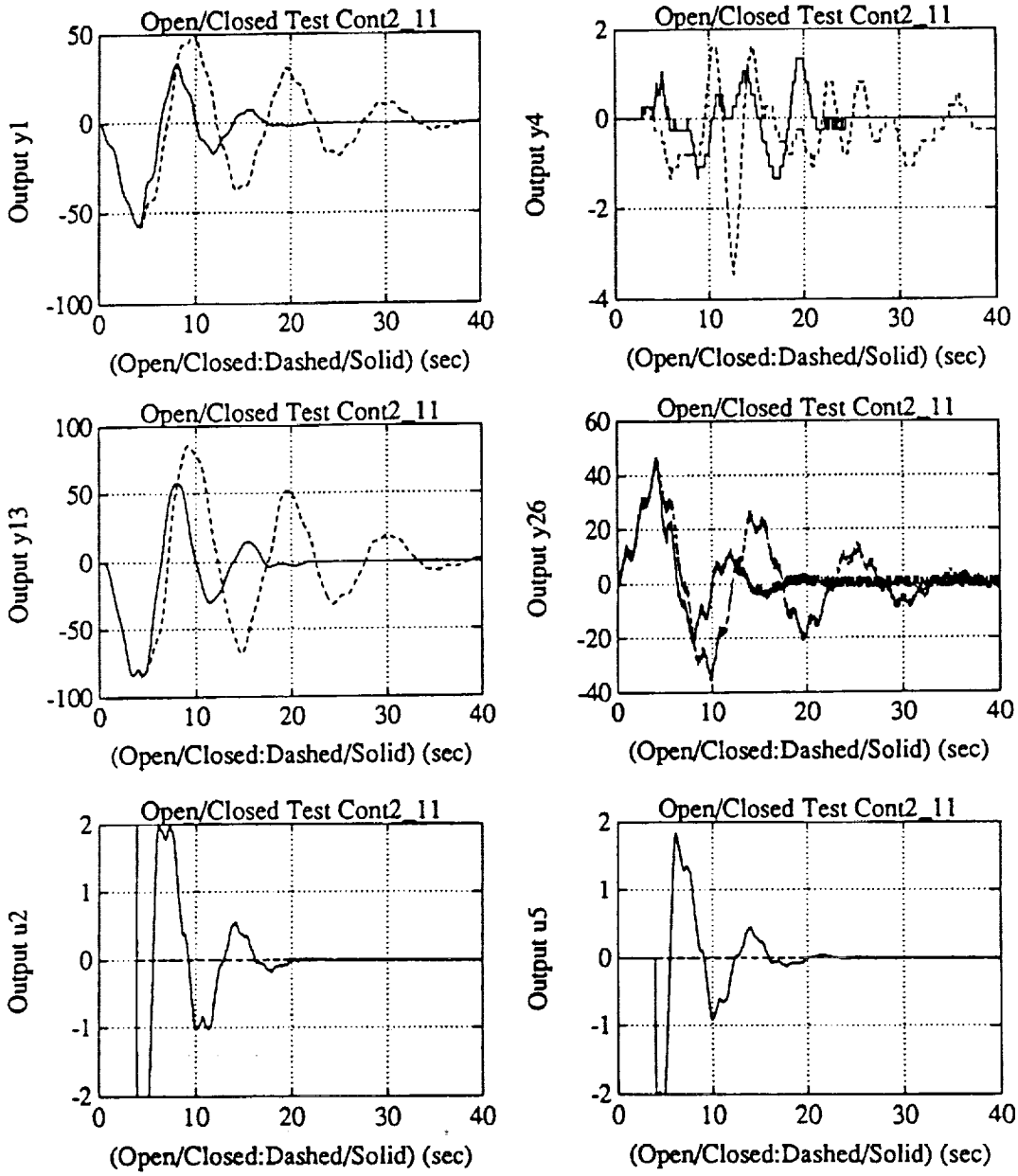


Figure 12 Y Direction Pulse Responses of the BOCC Design